

Short Communication

Effect of Surface Roughness on the Corrosion Behavior of Pure Iron in Acidic Solutions

Ahmed S. Alshamsi* and Afra AlBlooshi

Department of Chemistry, College of Science, United Arab Emirates University, Al Ain, UAE

*E-mail: a.alshamsi@uaeu.ac.ae

Received: 28 August 2018 / Accepted: 18 February 2019 / Published: 10 May 2019

The effect of surface roughness on the corrosion behavior of pure iron in acidic solutions (hydrochloric and sulfuric acids) in the absence and presence of molybdate ions was thoroughly investigated. Polarization techniques, electrochemical impedance spectroscopy, and scanning electron microscopy were used for this investigation. The results demonstrated that increasing surface roughness and the presence of molybdate ions have detrimental effects on the corrosion resistance of pure iron in acidic solutions. While general corrosion was observed at the open circuit potential, crystallographic pits were observed under anodic polarization in hydrochloric acid solutions.

Keywords: iron, corrosion, EIS, roughness, molybdate, HCl, H₂SO₄.

1. INTRODUCTION

Sulfuric and hydrochloric acids (H₂SO₄ and HCl, respectively) are widely used in the industry for pickling, cleaning, and descaling. Surface roughness and molybdate ions (MoO₄²⁻) are among the many factors affecting the corrosion behavior of metals and alloys. Environmentally friendly MoO₄²⁻ has been of interest as a corrosion inhibitor due to very low toxicity [1]. Alloying molybdenum (Mo) to steel is known to reduce steel's susceptibility to localized corrosion [2]. Interestingly, alloying Mo to the steel or adding MoO₄²⁻ has shown similar effects in terms of increasing the repassivation rate and enhancing resistance to localized corrosion [3–7]. It has been suggested that in acidic chloride-containing solutions, Mo may dissolve as MoO₄²⁻ and consequently react with iron (Fe) cations to form insoluble MoO₄²⁻ precipitates in these solutions. The precipitates result in hindrance of the transpassive reaction leading to lower current densities [6]. Furthermore, it can also be argued that the formation of an Mo-rich stable oxide film (MoO₃) in the outer region of the passive film is responsible for enhancing stainless steel corrosion resistance in acidic solutions [8]. However, a minimum concentration of 5 wt% Mo is

required in order to improve corrosion resistance in Fe-Mo alloys [3]. Furthermore, relatively low Mo and MoO_4^{2-} concentrations were reported to have detrimental effects on various metals' and alloys' resistance to corrosion [3, 9–13]. Moreover, it was reported that the presence of MoO_4^{2-} affects both passivity and pit nucleation by deactivating the sites at which pit formation occurs and by reducing the pit size. As a result, it is more difficult for pits to develop into stable ones [14]. Some argue that Mo improves stainless steel corrosion resistance by reducing the active dissolution rates of salt-free surfaces, leading to repassivation and termination of localized corrosion [15]. Others reported that alloyed Mo and MoO_4^{2-} inhibit metastable pitting [7]. Wang *et al.* concluded that the growth of stable Fe pits in the absence of sulfide inclusions was due to potential with the nucleation behavior similar to some carbon steels [16]. Burstein and Pistorius reported surface roughness affected pitting corrosion of 304 stainless steels with an increasing nucleation rate of metastable pits corresponding to an increase in surface roughness in solutions containing chloride ions [17].

Surface texture (preferred orientation) and surface roughness influence carbon steels' corrosion behavior [18]. Wang *et al.* reported an increase in charge transfer resistance (R_{ct}) values with decreasing roughness for mild steel tested in ammonium chloride (NH_4Cl) solution [19]. Viera *et al.* reported a decrease in pitting corrosion resistance with increasing roughness of the 316L and low carbon austenitic stainless steels tested in physiological solutions [20]. Interestingly, Toloei *et al.* reported that while the corrosion rate of nickel (Ni) in H_2SO_4 increased with increasing roughness, the corrosion rate of mild steel in H_2SO_4 decreased with increasing roughness [21]. Roxanna *et al.* reported a decrease in the corrosion rate corresponding to an increase in roughness for the AE44 magnesium alloy tested in aerated 3.5% sodium chloride (NaCl) solution [22].

Clearly, surface roughness and MoO_4^{2-} affect the corrosive behavior of metals and alloys. However, the nature of such effects, such as increasing/decreasing the corrosion rate, depends on the type of material and MoO_4^{2-} concentration.

While it is generally accepted that relatively high concentrations of Mo and MoO_4^{2-} inhibit corrosion, there is no widely accepted mechanism on the way in which Mo or MoO_4^{2-} enhance corrosion resistance. Pure Fe, unlike steel, does not contain sulfide inclusions. Consequently, the effects of inclusions on corrosion mechanisms and rates and on nucleation and pit growth can be excluded. As a result, nucleation and pit growth (when it occurs) can be related to surface roughness. The main objective of this study was to investigate the effects of surface roughness on Fe's corrosion behavior in two different acids (H_2SO_4 and HCl), one of them containing chloride. In addition, the role of MoO_4^{2-} as a corrosion inhibitor was investigated as a function of surface roughness.

2. EXPERIMENTS

Commercial Fe (99.99+ %) was tested in 0.1 M H_2SO_4 and in 0.1 M HCl solutions in the absence and presence of MoO_4^{2-} at $22\text{ }^\circ\text{C} \pm 1\text{ }^\circ\text{C}$. An Fe rod, 2 mm in diameter, was coated with epoxy, but the cross-sectional area (0.0314 cm^2) was exposed to the testing solution. The sample was wet-ground using only grit paper P120 in order to maintain a relatively rough surface area. Alternatively, the sample was wet-ground using P120 followed by P280, P400, P800, and finally with P1200 in order to maintain a

relatively smooth surface area. The sample was cleaned with distilled water and placed in a 3-electrode cell with platinum (Pt) as a counter-electrode and saturated Ag/AgCl electrode as the reference electrode, +0.197 V versus the standard hydrogen electrode (SHE). Standard corrosion techniques include the open circuit potential versus time (OCP versus t), polarization resistance versus time (R_p versus t), potentiodynamic polarization, potentiostatic polarization, and electrochemical impedance spectroscopy (EIS) measurements. Different potentiodynamic polarization measurements were conducted: (1) one set of potentiodynamic polarization measurements were initiated at -250 mV versus the corrosion potential (E_c) to $+250$ mV using a scanning rate of 0.167 mV s^{-1} and (2) the other polarization measurements were initiated at $+250$ mV versus an E_c to $+750$ mV using a scanning rate of 0.1 mV s^{-1} . The R_p versus t measurements were conducted at a scanning rate of 0.1 mV s^{-1} with experiments conducted at ± 10 mV versus E_c . Six data points were collected per R_p versus t experiment. Each set of two points were separated by a 5-min time interval. The potentiostatic experiments were conducted in 0.1 M HCl and in 0.1 M HCl + 0.01 M Na_2MoO_4 at an applied potential of about $+1000$ mV above E_c . The applied potential is sufficiently high in order to allow for pitting to occur. No potentiostatic experiments were conducted in 0.1 M H_2SO_4 solution because the solution does not cause pitting. EIS experiments were conducted using an applied alternating current (AC) potential of 10 mV with frequencies ranging from 0.005 to $100,000$ Hz. Magnetic stirring at a constant rate was maintained in all experiments. Each experiment started with OCP monitoring for 1 h followed by R_p versus t, EIS, and finally potentiostatic or potentiodynamic polarization measurements. The solution was purged with high purity nitrogen gas throughout the experiment. Data were collected automatically with the aid of a potentiostat/galvanostat (Gamry G750). All data analyses and extrapolations were performed using Gamry corrosion software (Gamry Echem Analyst). On average, three independent experiments were conducted for all specimens. The samples' surface morphologies were examined using scanning electron microscopy (SEM). The samples were cleaned in an ultrasound bath for a few minutes prior to SEM examination.

3. RESULTS AND DISCUSSIONS

Figure 1 (a, b) provides SEM micrographs of the polished smooth (P1200) and the rough (P120) surface, respectively. Figure 2 (a, b) shows the R_p versus t for Fe tested in 0.1 M HCl and 0.1 M HCl + 0.01 M Na_2MoO_4 as a function of surface roughness. Both figures show lower R_p values for the rough versus the smooth surface. Furthermore, when comparing the two figures, the presence of MoO_4^{2-} lowered the R_p values samples with the same surface roughness. The corrosion current density, which represents the corrosion rate, is given by the well-known formula $i_c = B/R_p$ in which B is a constant represented by $B = \beta_a \beta_c / [2.3(\beta_a + \beta_c)]$ in which β_a and β_c are the anodic and cathodic Tafel slopes extrapolated from the polarization curves, respectively. Hence, the presence of MoO_4^{2-} caused an increase in the corrosion rate. Clearly, MoO_4^{2-} acted as a corrosion accelerator instead of a corrosion inhibitor under the applied conditions.

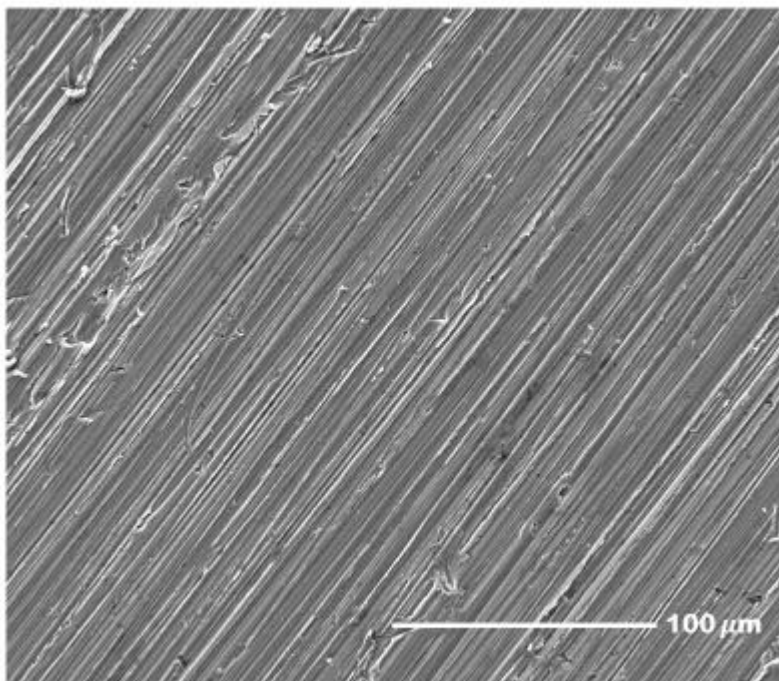


Figure 1(a). SEM micrograph of polished Fe surface with smooth finish (P1200).

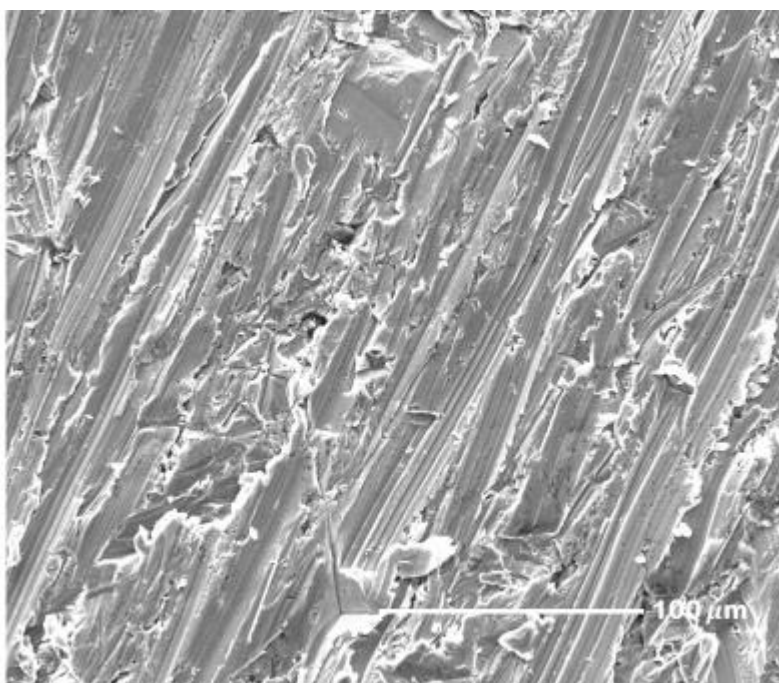


Figure 1(b). SEM micrograph of polished Fe surface with rough finish (P120).

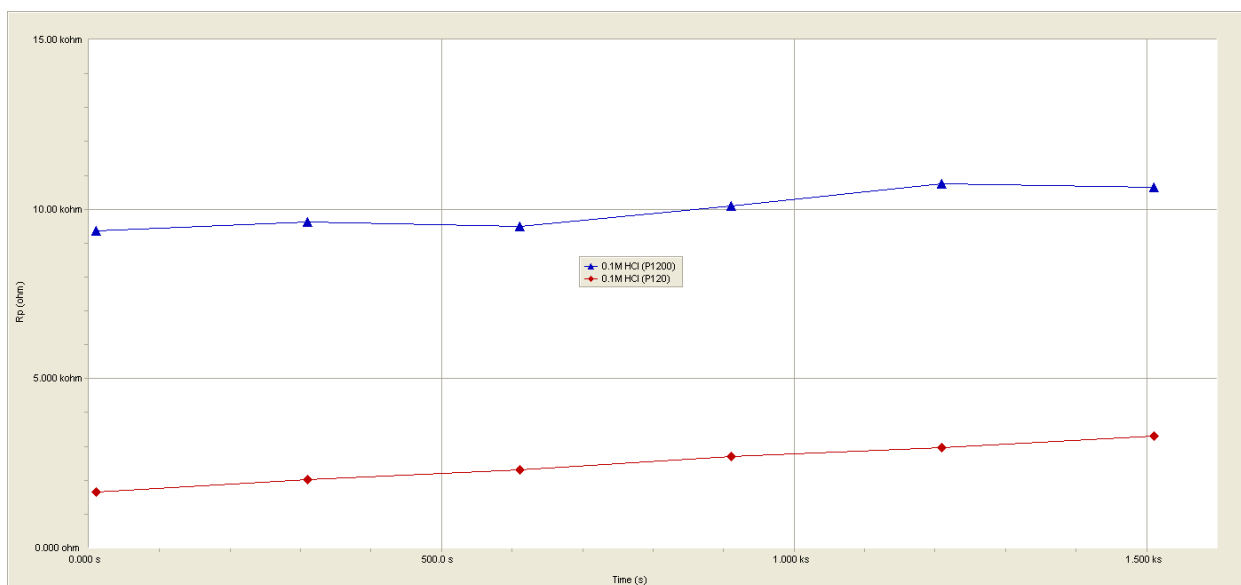


Figure 2a. R_p versus t measurements of Fe tested in 0.1 M HCl as a function of surface roughness.

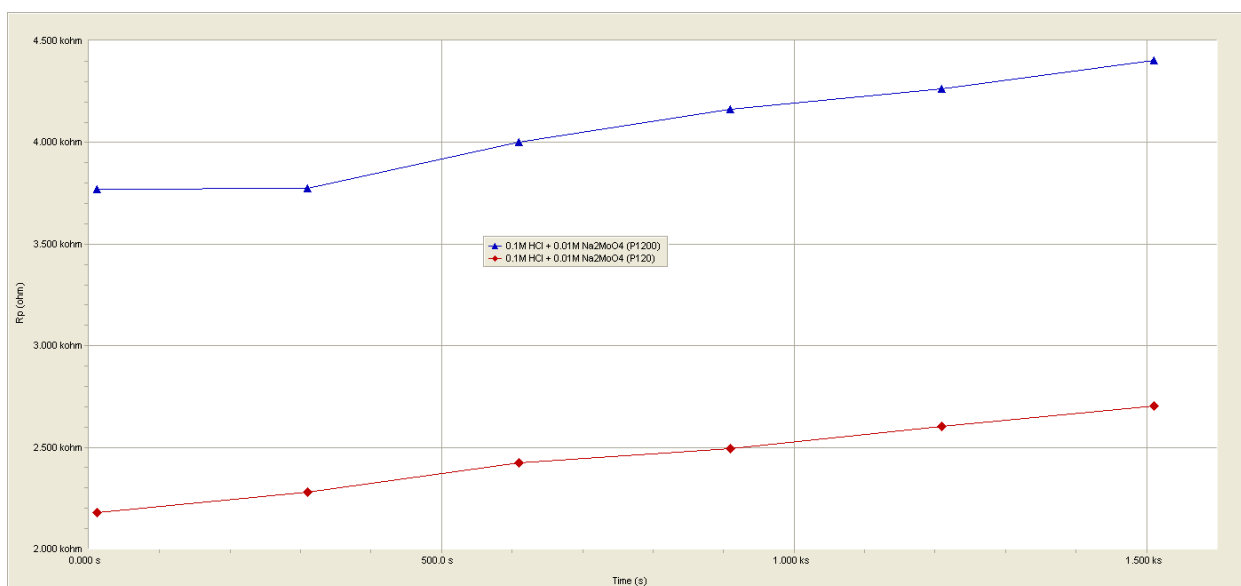


Figure 2b. R_p versus t measurements of Fe tested in 0.1 M HCl + 0.01 M Na_2MoO_4 as a function of surface roughness.

Figure 3 (a, b) shows R_p versus t for Fe tested in both 0.1 M H_2SO_4 and in 0.1 M H_2SO_4 + 0.01 M Na_2MoO_4 as a function of surface roughness. The corrosion behavior of Fe in these solutions follows the same trend as Fe in HCl solutions. The decrease in R_p values in the presence of MoO_4^{2-} should not be surprising since similar behaviors have been reported for 304 stainless steels in the presence of chloride ions [9].

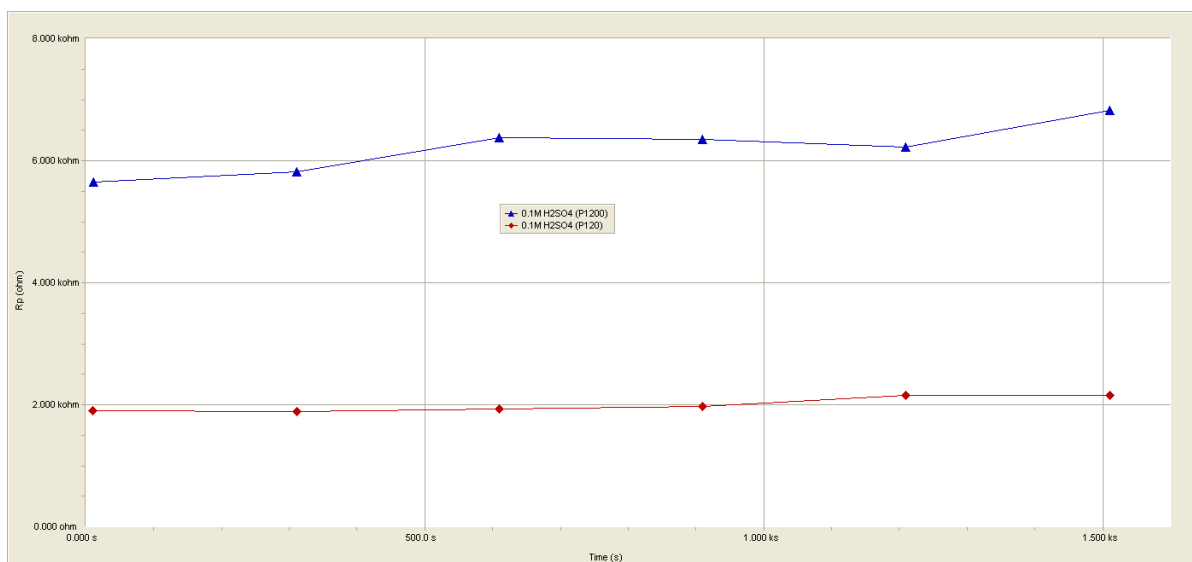


Figure 3a. R_p versus t measurements of Fe tested in 0.1 M H_2SO_4 as a function of surface roughness.

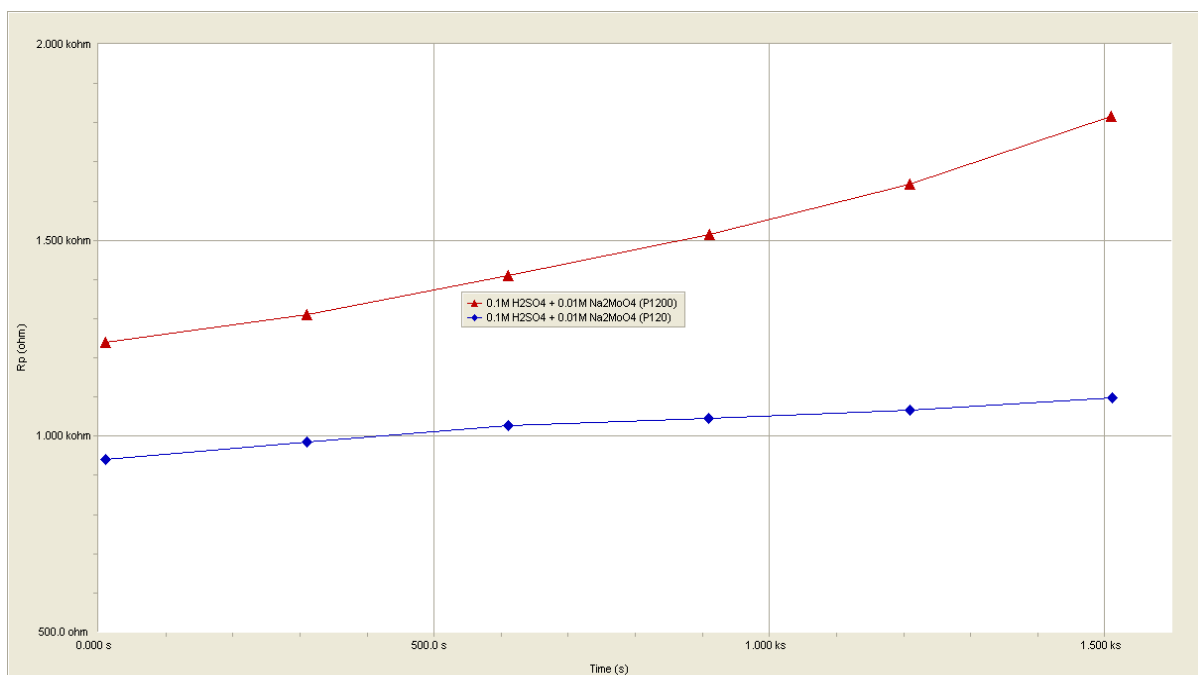


Figure 3b. R_p versus t measurements of Fe tested in 0.1 M H_2SO_4 + 0.01 M Na_2MoO_4 as a function of surface roughness.

Figure 4 (a, b) shows the potentiodynamic polarization curves for Fe in 0.1 M HCl and in 0.1 M HCl + 0.01 M Na_2MoO_4 as a function of surface roughness, respectively. Figure 5 (a, b) shows similar potentiodynamic polarization curves for Fe in 0.1 M H_2SO_4 and Fe in 0.1 M H_2SO_4 + 0.01M Na_2MoO_4 as a function of surface roughness, respectively.

The corrosion potential, E_c , and the corrosion current densities, i_c , extrapolated from the polarization curves, are reported in Table 1 along with the R_p values obtained from the R_p versus t

measurements. The data correlates well; the higher the R_p , the lower the i_c . The $\%R_p$ change is calculated using the equation:

$$\% R_p \text{ change} = (R_p[\text{smooth}] - R_p[\text{rough}]) / R_p [\text{rough}] \times 100\%$$

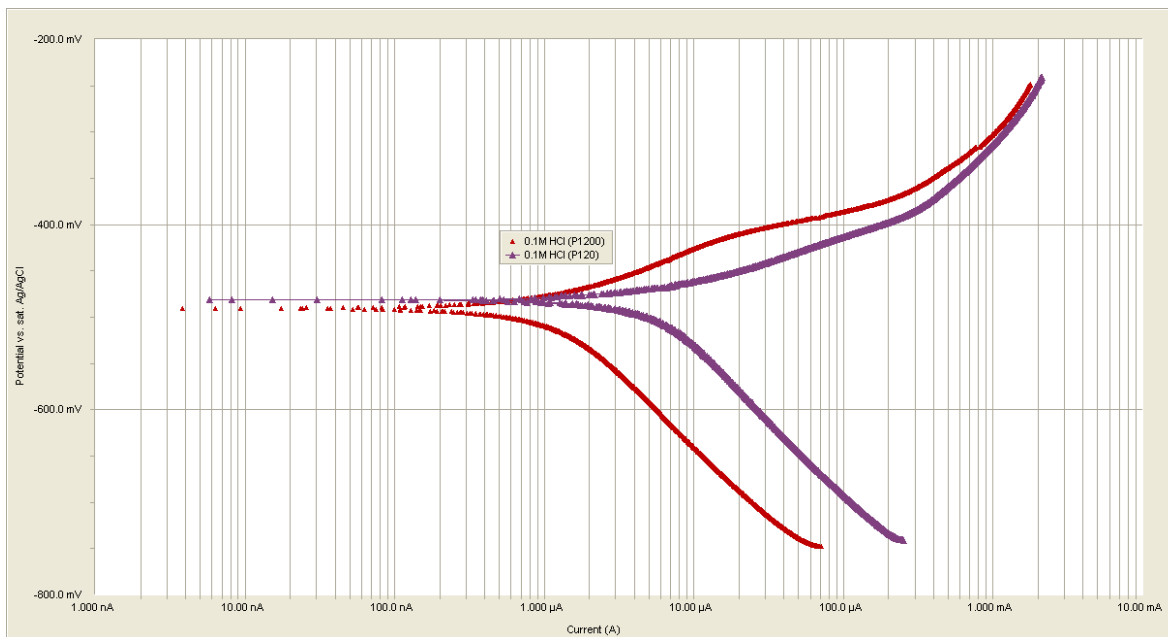


Figure 4a. Potentiodynamic polarization curves of Fe in 0.1M HCl as a function of surface roughness.

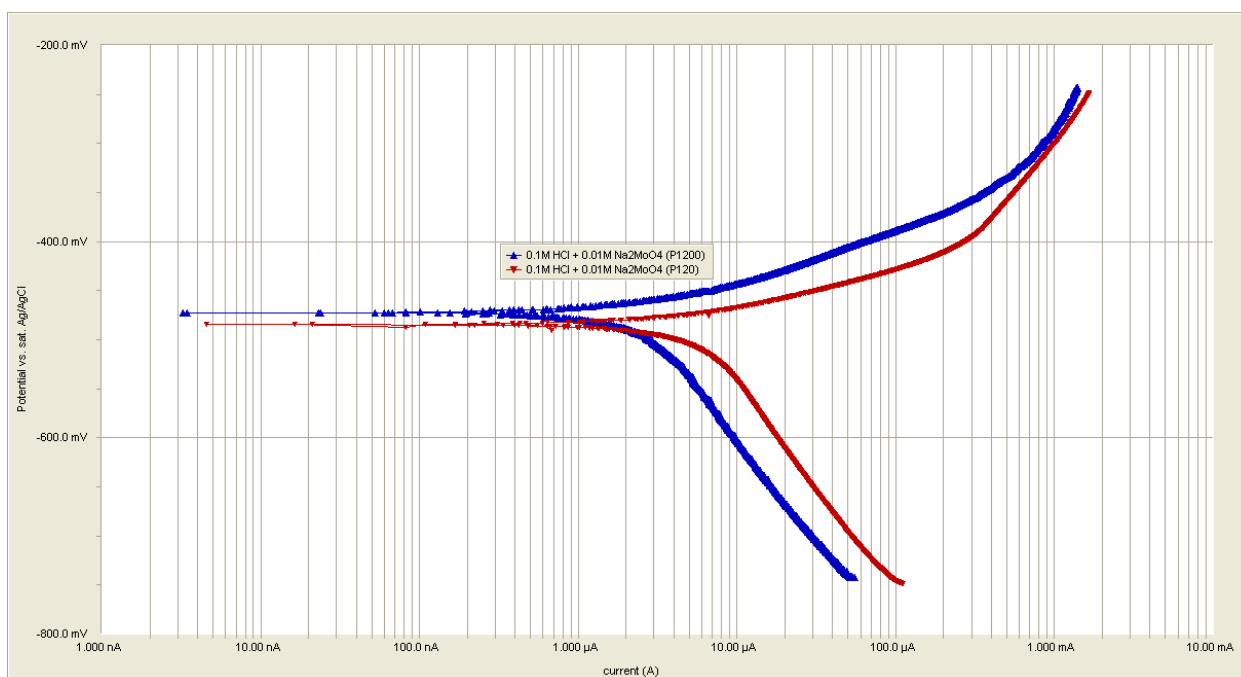


Figure 4b. Potentiodynamic polarization curves of Fe in 0.1 M HCl + 0.01 M Na_2MoO_4 as a function of surface roughness.

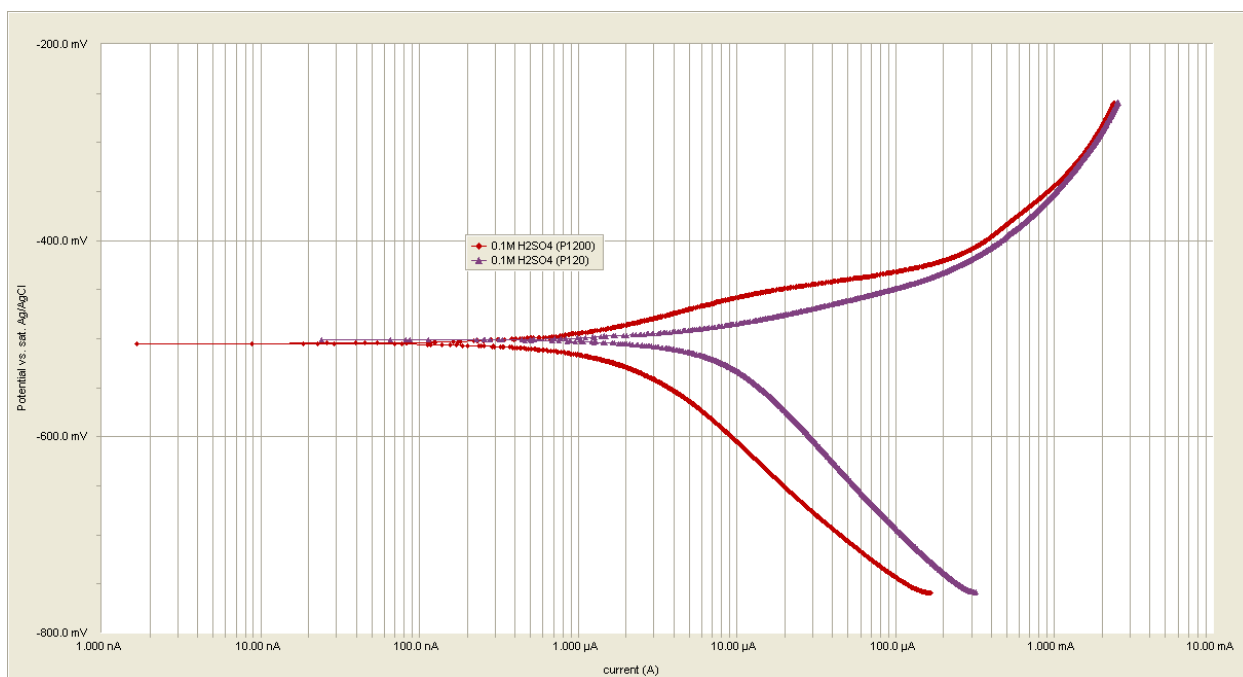


Figure 5a. Potentiodynamic polarization curves of Fe in 0.1 M H₂SO₄ as a function of surface roughness.

In order to further investigate Fe’s corrosion behavior in the two solutions, *EIS* measurements were conducted. The Nyquist plots of Fe in 0.1 M HCl and in 0.1 M H₂SO₄ are given in Figures 6 (a, b) and 7 (a, b), respectively. Inspection of Figures 6 and 7 shows the existence of depressed single semicircles with different diameters and degrees of depression. The single semicircle represents a single charge transfer process, while a depressed semicircle depicts surface roughness or inhomogeneity [23, 24]. The R_p value can be estimated from the semicircle’s diameter [23].

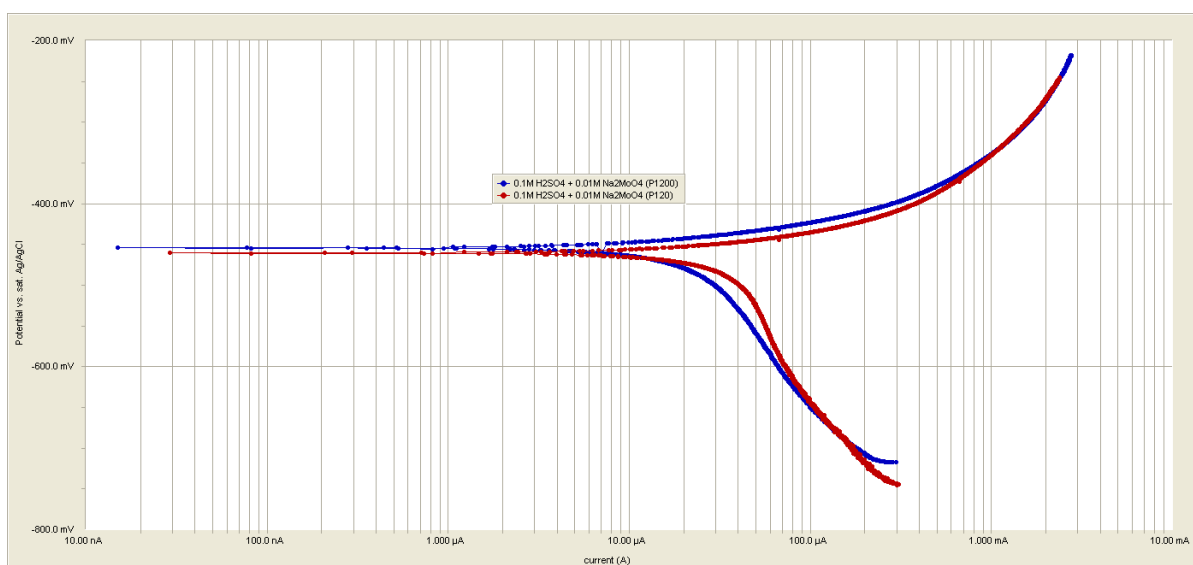


Figure 5b. Potentiodynamic polarization curves of Fe in 0.1 M H₂SO₄ + 0.01 M Na₂MoO₄ as a function of surface roughness.

Table 1. Electrochemical parameters of Fe in 0.1 M H₂SO₄ and 0.1 M HCl as a function of surface roughness in the absence and presence of MoO₄²⁻.

Solution	E_c (mV)	R_p (Ω cm ²)	i_c (μ A cm ²)	% R_p change with roughness
0.1 M H ₂ SO ₄ (P1200)	-503 ± 3.2	169.9 ± 55.5	44.5 ± 2.3	+178
0.1 M H ₂ SO ₄ (P120)	-502 ± 2.2	61.1 ± 13.6	203.7 ± 37.2	-
0.1 M H ₂ SO ₄ + 0.01M Na ₂ MoO ₄ (P1200)	-475 ± 18.8	34.7 ± 5.5	865.2 ± 156.8	+4.8
0.1 M H ₂ SO ₄ + 0.01M Na ₂ MoO ₄ (P120)	-460 ± 9.0	33.1 ± 6.5	1420.4 ± 631	-
0.1 M HCl (P1200)	-500 ± 8.72	394.3 ± 81.2	61.9 ± 15.6	+474.8
0.1 M HCl (P120)	-482 ± 5.77	68.6 ± 10.6	142.5 ± 41.8	-
0.1 M HCl + 0.01 M Na ₂ MoO ₄ (P1200)	-467 ± 8.5	138.1 ± 75.2	118.8 ± 25.5	+117.1
0.1 M HCl + 0.01 M Na ₂ MoO ₄ (P120)	-479 ± 8.5	63.6 ± 18.0	182.6 ± 38.8	-

Inspection of Figures 6 and 7 clearly reveals that the smooth surfaces depict larger diameters (larger impedance) and consequently higher R_p values in comparison to the rough surfaces. Table 2 shows the *EIS* parameters calculated using the constant phase element (CPE) circuit used to fit the Nyquist plots in Figures 6 and 7. The CPE circuit is shown in Figure 8. The R_p data from *EIS*, reported in Table 2, generally follows the same trend as those from R_p versus *t* measurements and are reported in Table 1.

CPE is defined by the equation [25]:

$$Z(\text{CPE}) = Y_0^{-1} (j\omega)^{-\alpha}$$

in which Y_0 is the CPE constant, ω is the angular frequency in rad s⁻¹, $j^2 = -1$ is the imaginary number, and α is the CPE exponent.

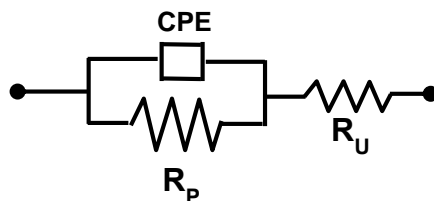


Figure 8. The equivalent circuit is used to fit the *EIS* data. (CPE the constant phase element, R_p the polarization resistance, and the R_u the solution resistance).

The physical interpretation of the CPE depends on the value of α . CPE represents resistance ($Z[\text{CPE}] = R, \alpha = 0$), capacitance ($Z[\text{CPE}] = C, \alpha = 1$), inductance ($Z[\text{CPE}] = L, \alpha = -1$), or Warburg impedance for ($\alpha = 0.5$). The CPE is considered a capacitor when values of α are ≥ 0.8 . In the current study, the α values range from about 0.70 to 0.86. Deviation from an ideal capacitor ($\alpha = 1$) can be attributed to heterogeneity and roughness. The α values in Table 2 show higher α values for the smooth surface rather than the rough surface and higher α values in H_2SO_4 solutions rather than in the HCl solutions. The lower α values in the HCl solutions can be attributed to the aggressive nature of the HCl , which is known to cause localized corrosion.

Table 2: Electrochemical impedance parameters of Fe in 0.1 M HCl and 0.1 M H_2SO_4 as a function of surface roughness in the absence and presence of MoO_4^{2-} .

Solution	R_p ($\Omega \text{ cm}^2$)	R_u ($\Omega \text{ cm}^2$)	Y_o ($\Omega^{-1} \text{ cm}^{-2} \text{ s}^\alpha$)	α	% R_p change with roughness
0.1 M H_2SO_4 (P1200)	248.47 ± 1.30	1.69 ± 0.0127	$1.67 \times 10^{-4} \pm 3.0 \times 10^{-6}$	0.857	+253.5%
0.1 M H_2SO_4 (P120)	70.08 ± 0.362	1.65 ± 0.0115	$3.86 \times 10^{-4} \pm 8.98 \times 10^{-6}$	0.840	-
0.1 M H_2SO_4 + 0.01M Na_2MoO_4 (P1200)	31.58 ± 0.164	2.103 ± 0.0144	$3.18 \times 10^{-4} \pm 1.37 \times 10^{-5}$	0.837	-33.88%
0.1 M H_2SO_4 + 0.01M Na_2MoO_4 (P120)	47.76 ± 0.276	2.040 ± 0.0131	$1.19 \times 10^{-3} \pm 2.84 \times 10^{-5}$	0.780	-
0.1 M HCl (P1200)	285.20 ± 1.57	2.032 ± 0.0159	$2.64 \times 10^{-5} \pm 4.50 \times 10^{-6}$	0.789	+298.5%
0.1 M HCl (P120)	71.561 ± 0.464	1.761 ± 0.0121	$2.40 \times 10^{-3} \pm 4.34 \times 10^{-5}$	0.697	-
0.1 M HCl + 0.01M Na_2MoO_4 (P1200)	173.59 ± 1.075	3.319 ± 0.0219	$8.38 \times 10^{-4} \pm 1.47 \times 10^{-5}$	0.746	+81.2%
0.1 M HCl + 0.01M Na_2MoO_4 (P120)	95.80 ± 0.599	3.033 ± 0.0188	$1.37 \times 10^{-3} \pm 2.64 \times 10^{-5}$	0.754	-

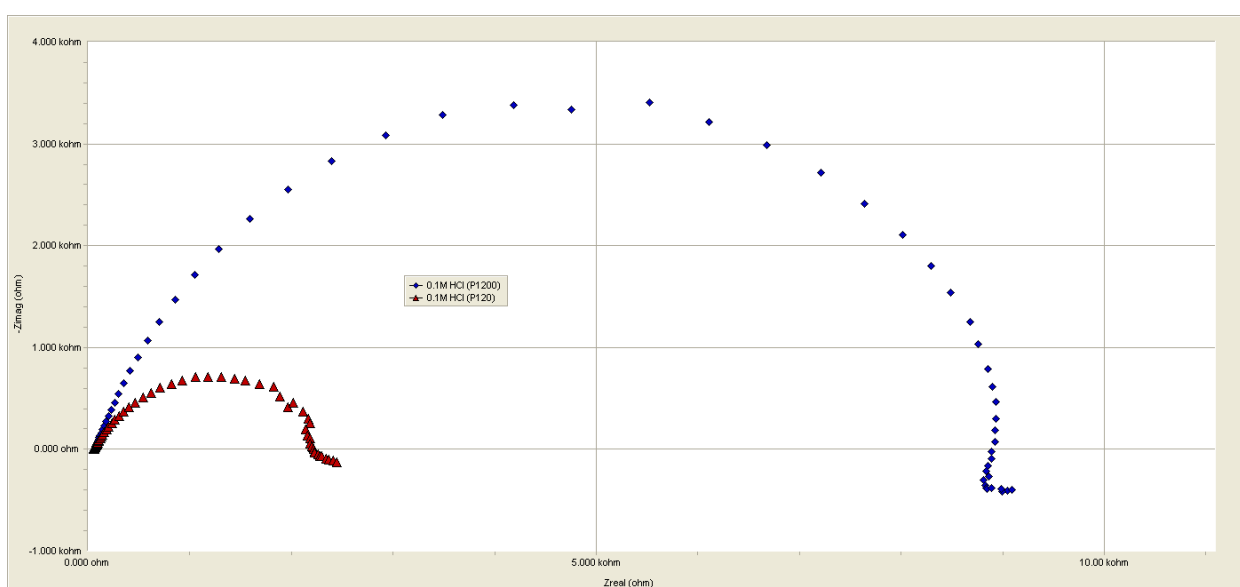


Figure 6a. Nyquist plots of Fe in 0.1 M HCl as a function of surface roughness.

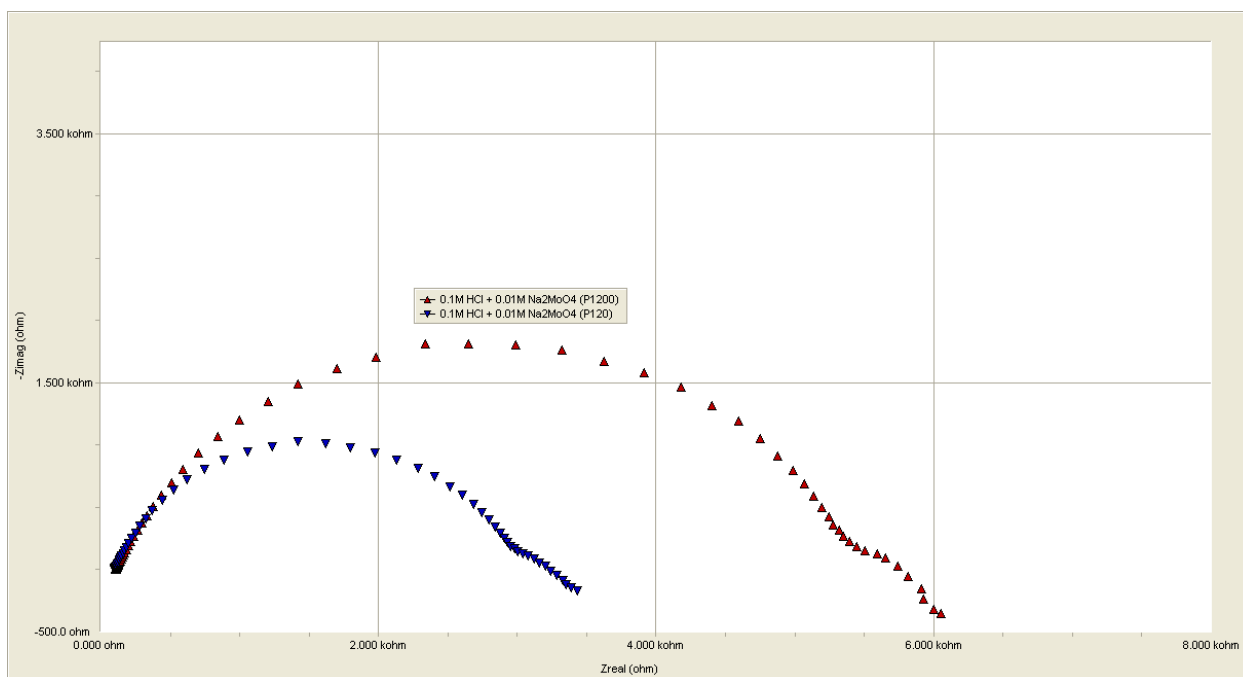


Figure 6b. Nyquist plots of Fe in 0.1 M HCl + 0.01 M Na₂MoO₄ as a function of surface roughness.

In order to investigate pitting corrosion, the Fe electrode was anodically polarized to 500 mV above the E_c. Figures 9 and 10 are the potentiodynamic anodic polarization curves for Fe in MoO₄²⁻ absence and presence, respectively. Figure 9 shows current transients that increased in frequency and size with increasing potential for both surfaces.

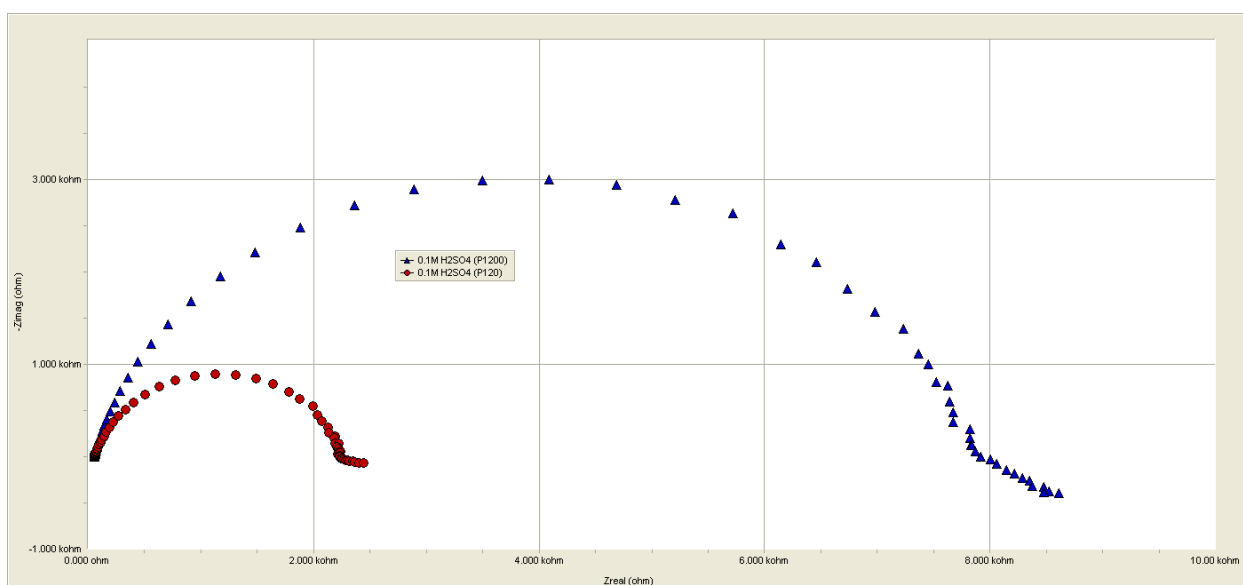


Figure 7a. Nyquist plots of Fe in 0.1 M H₂SO₄ as a function of surface roughness.

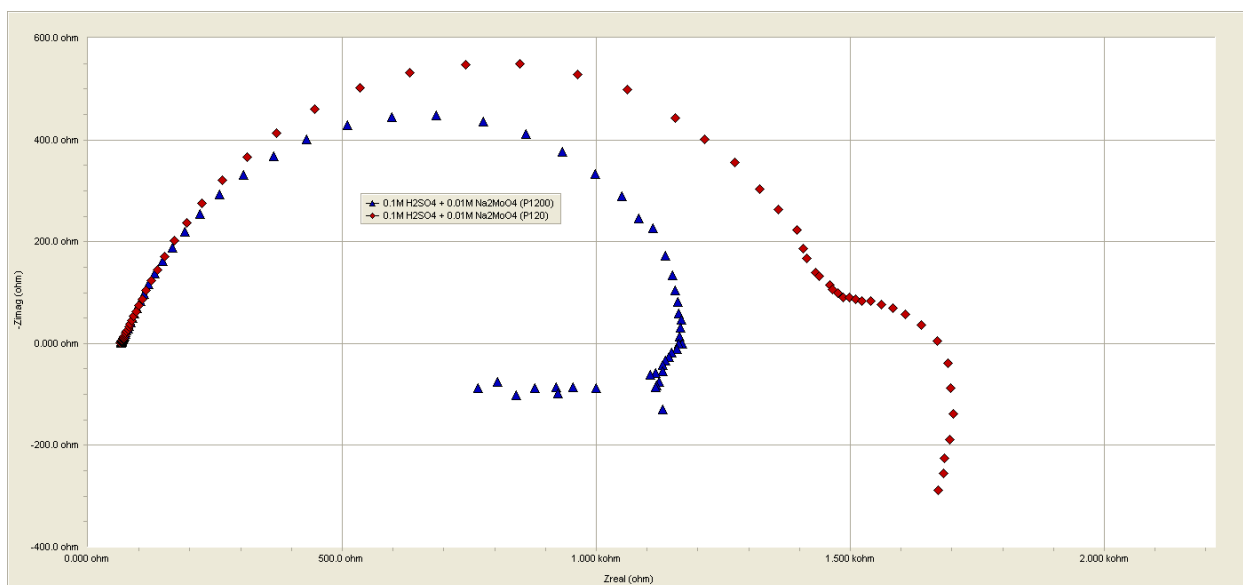


Figure 7b. Nyquist plots of Fe in 0.1 M H₂SO₄ + 0.01 M Na₂MoO₄ as a function of surface roughness.

These transients indicate metastable pit nucleation [14]. Moreover, the increase in current with increasing potential indicates the pits grew into stable ones. MoO₄²⁻ presence clearly caused a reduction in the current transients as shown in Figure 10. Nevertheless, the current continued to increase with an increase in potential.

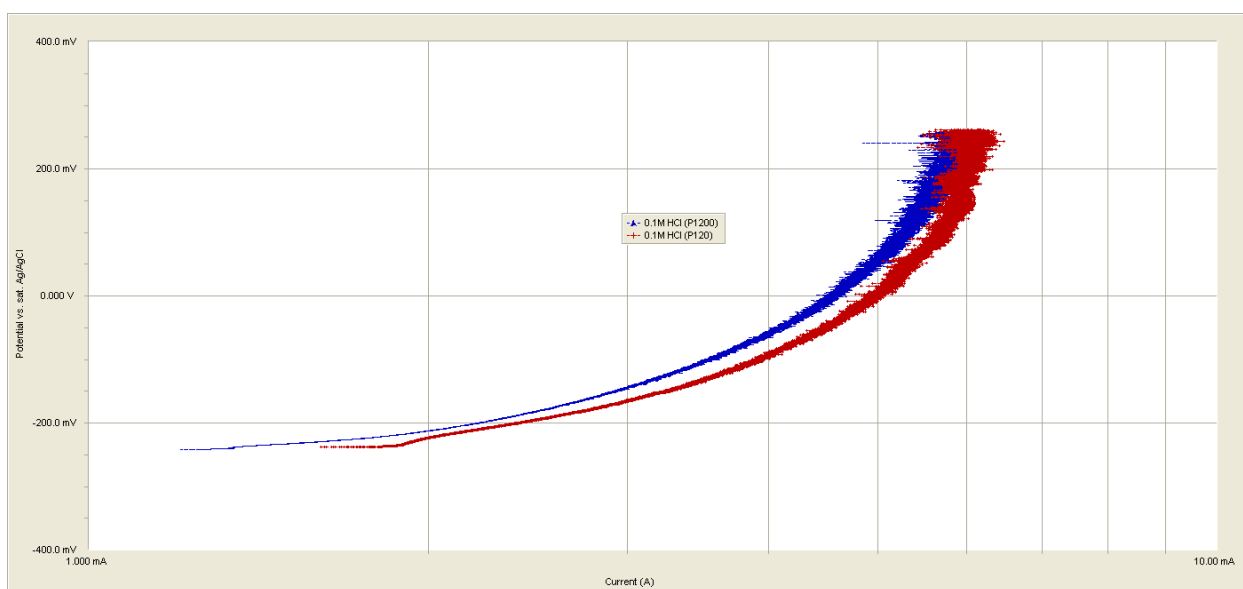


Figure 9. Potentiodynamic anodic polarization curves of Fe in 0.1 M HCl as a function of surface roughness.

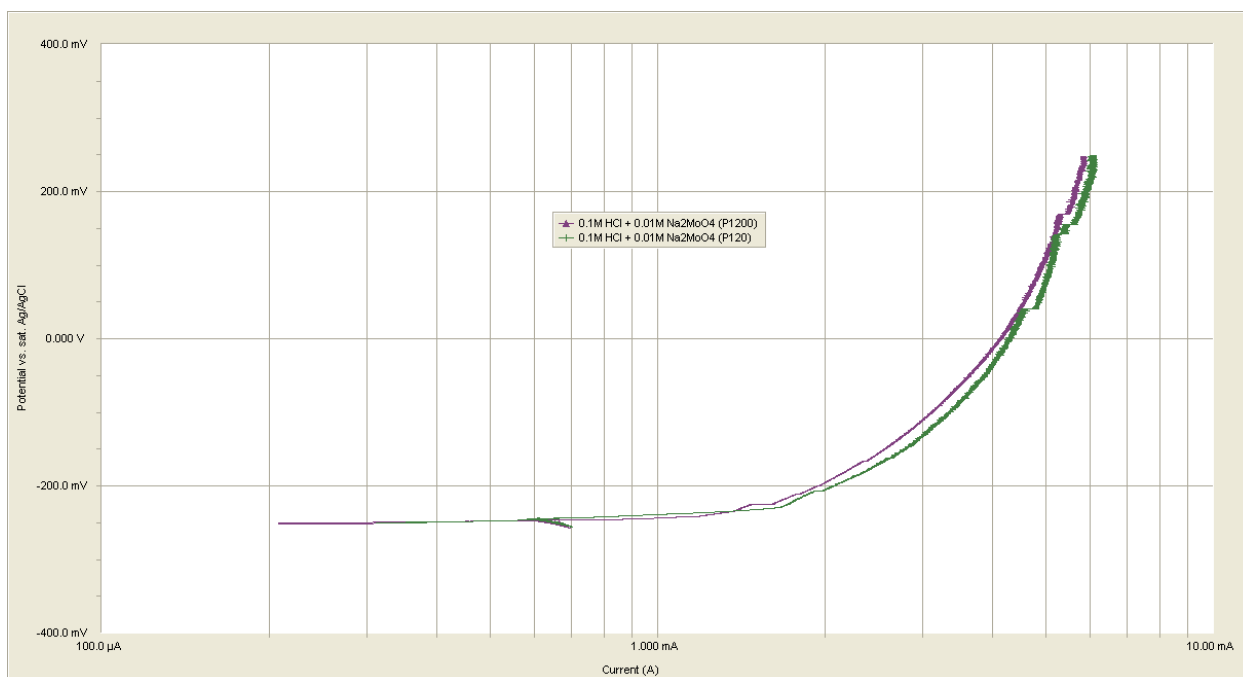


Figure 10. Potentiodynamic anodic polarization curves of Fe in 0.1 M HCl + 0.01 M Na₂MoO₄ as a function of surface roughness.

Figure 11 shows the potentiostatic anodic polarization curves for Fe in 0.1M HCl as a function of surface roughness under applied potential of about 1000 mV above E_c. Figure 12 shows the anodic potentiostatic polarization curves in the presence of MoO₄²⁻. The curves in Figure 12 clearly show that the presence of MoO₄²⁻ caused a decrease in the current and fluctuations when compared to current values in Figure 11 in which MoO₄²⁻ is absent. More importantly, the curves in Figures 11 and 12 do not show any signs of current decrease over time. Such behavior indicates that once pits form, they do not repassivate.

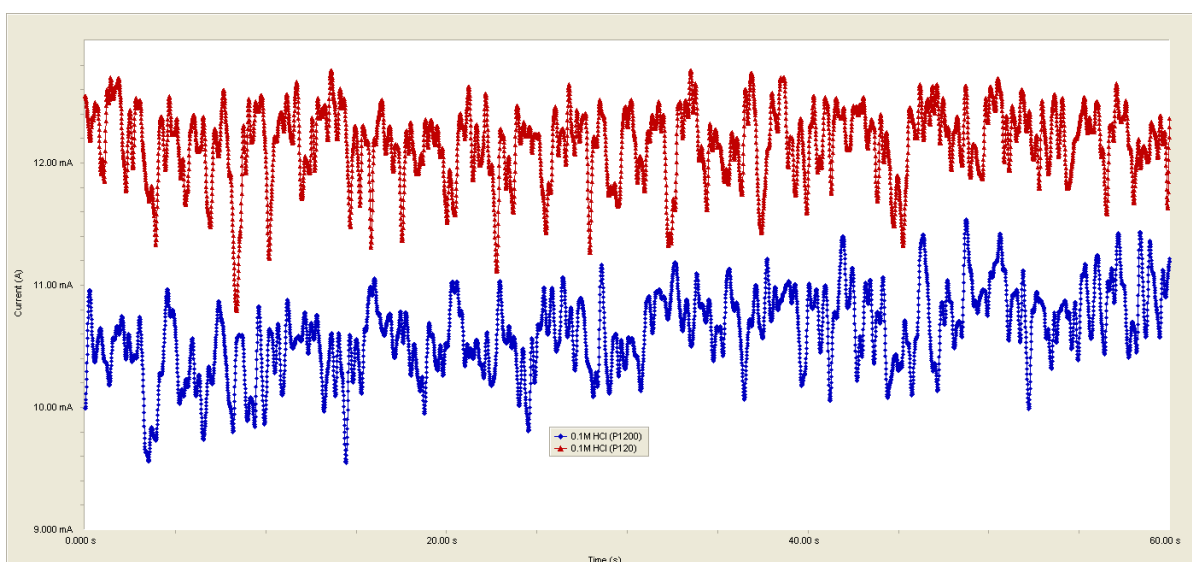


Figure 11. Potentiostatic anodic polarization curves of Fe in 0.1 M HCl as a function of surface roughness, E_{applied} = +1000 mV.

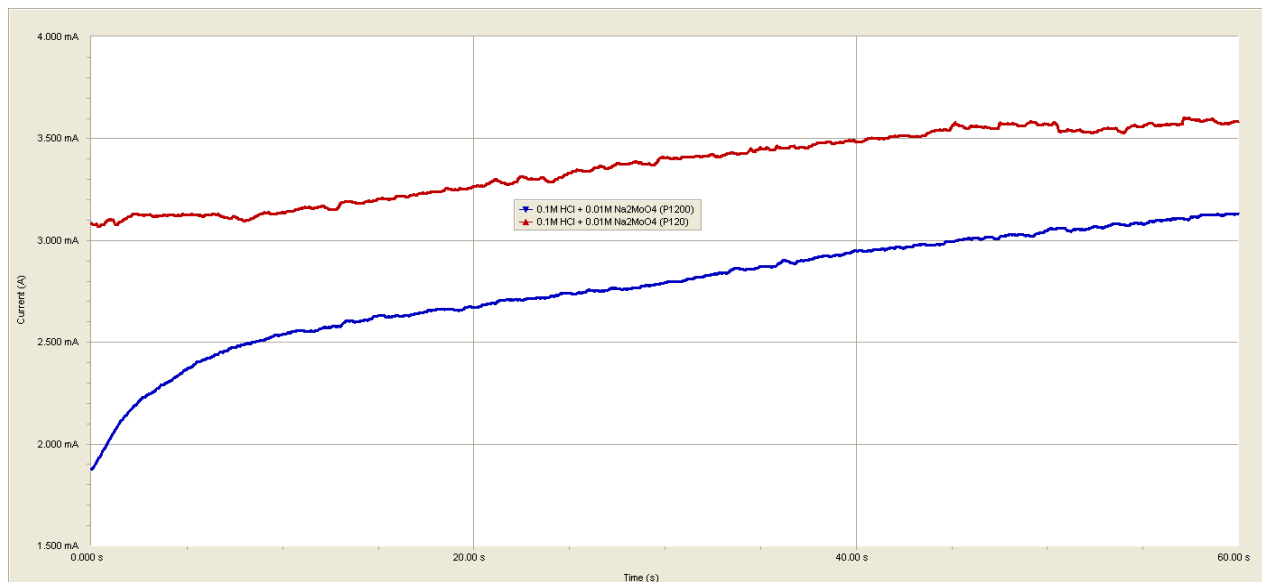


Figure 12. Potentiostatic anodic polarization curves of Fe in 0.1 M HCl + 0.1 M Na₂MoO₄ as a function of surface roughness, $E_{\text{applied}} = +1000$ mV.

Figure 13 shows the surface morphologies of Fe surfaces in 0.1 M HCl solution under different conditions. Figure 13 (a-d) show Fe surface morphologies in 0.1 M HCl in either MoO₄²⁻ absence and presence at the OCP. Only general corrosion with no signs of localized (pitting) corrosion was observed. Pits appeared when Fe was anodically polarized to a high potential (1000 mV above E_c) as shown in Figure 13 (e-h). Inspection of the micrographs shows the pits have random distribution. Moreover, the pits are deep and crystallographic.

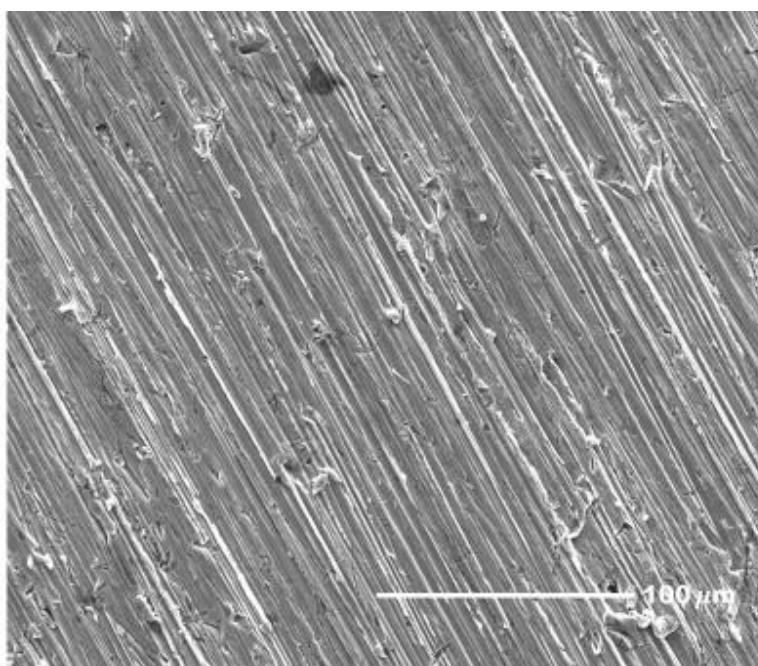


Figure 13(a): SEM micrograph of Fe (*smooth, P1200*) after one hour of immersion in 0.1 M HCl at the open circuit potential (OCP).

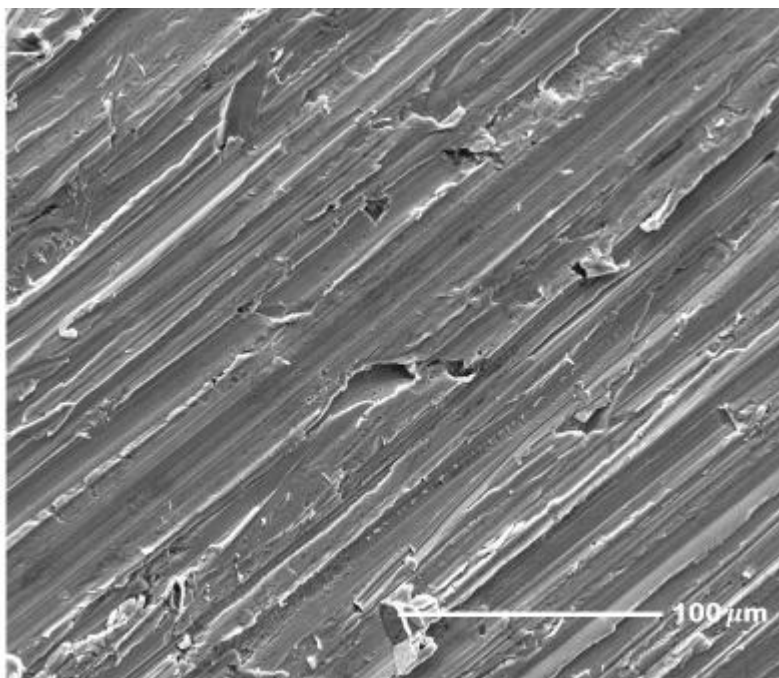


Figure 13(b): SEM micrograph of Fe (*rough, P120*) after one hour of immersion in 0.1M HCl at the OCP.

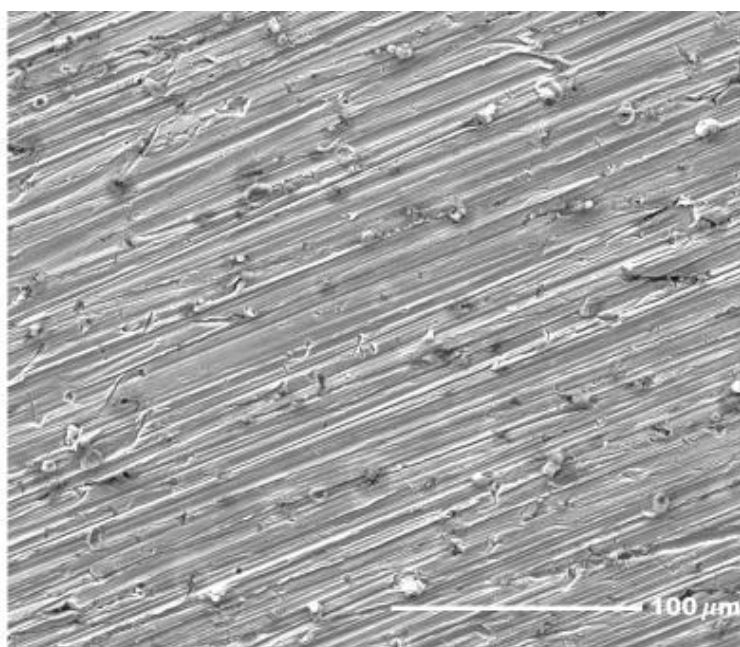


Figure 13(c): SEM micrograph of Fe (*smooth, P1200*) after one hour of immersion in 0.1M HCl + 0.01M Na₂MoO₄ at the OCP.

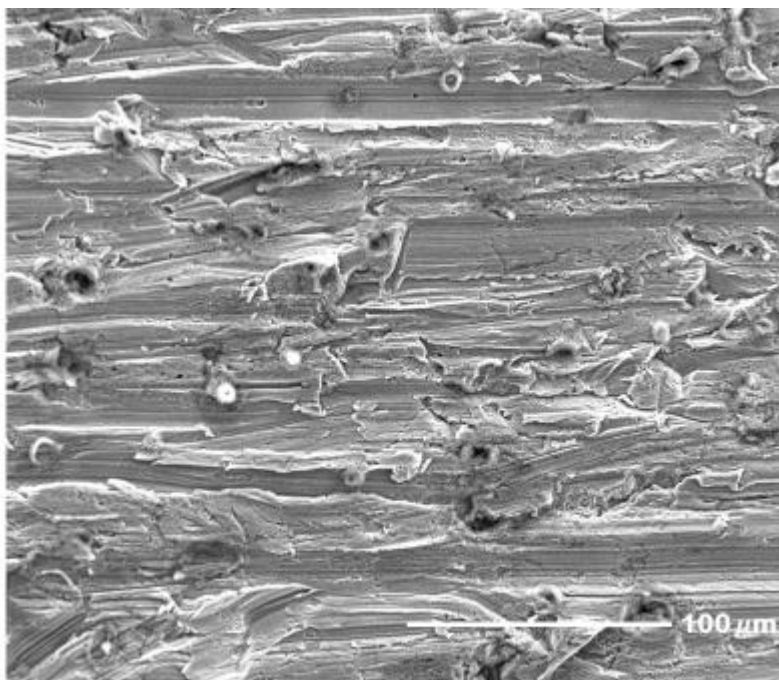


Figure 13(d): SEM micrograph of Fe (*rough, P120*) after one hour of immersion in 0.1M HCl + 0.01M Na₂MoO₄ at the OCP.

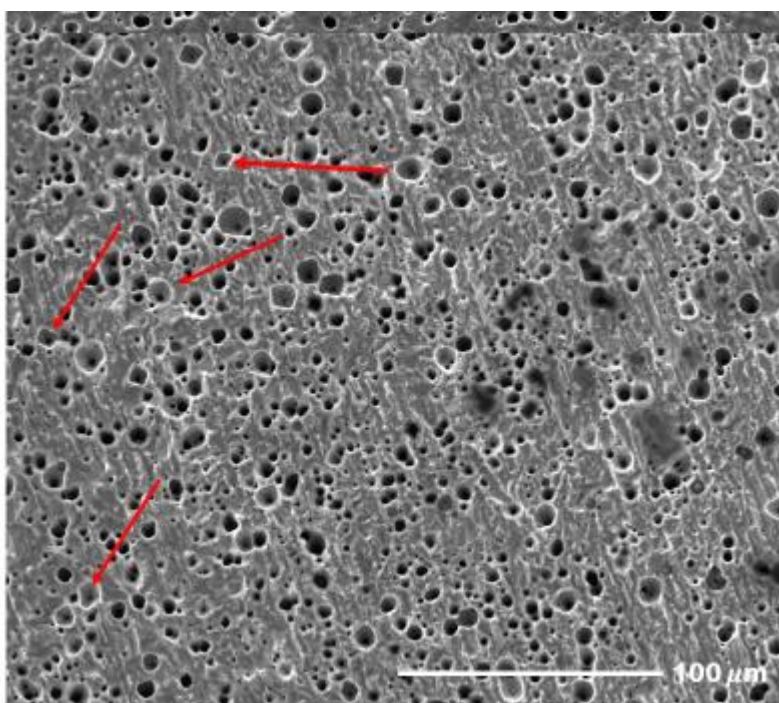


Figure 13(e): SEM micrograph of Fe (*smooth, P1200*) after one hour of immersion in 0.1 M HCl followed by an applied potential of 1000 mV above E_c for 60 seconds.

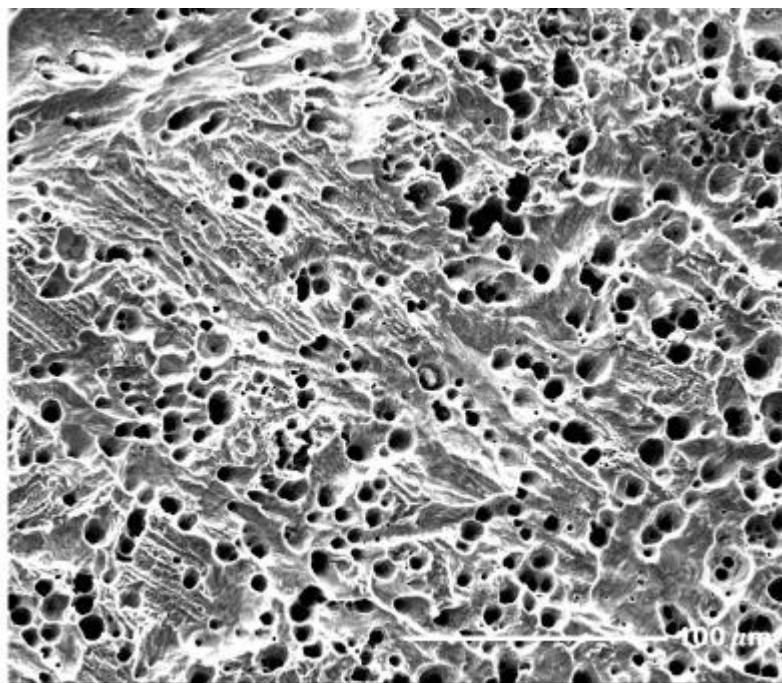


Figure 13(f): SEM micrograph of Fe (*rough, P120*) after one hour of immersion in 0.1M HCl followed by an applied potential of 1000 mV above E_c for 60 seconds.

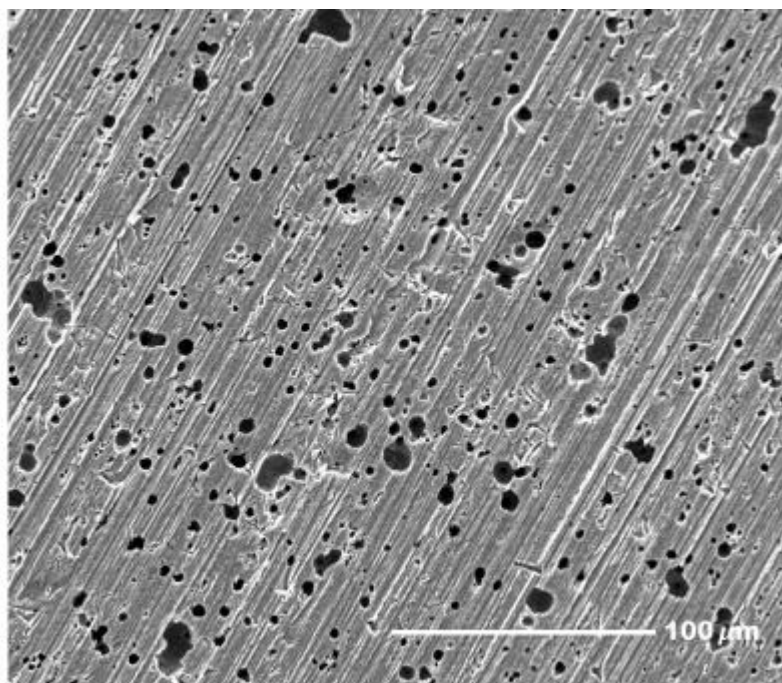


Figure 13(g): SEM micrograph of Fe (*smooth, P1200*) after one hour of immersion in 0.1 M HCl + 0.01 M Na_2MoO_4 followed by an applied potential of 1000 mV above E_c for 60 seconds.

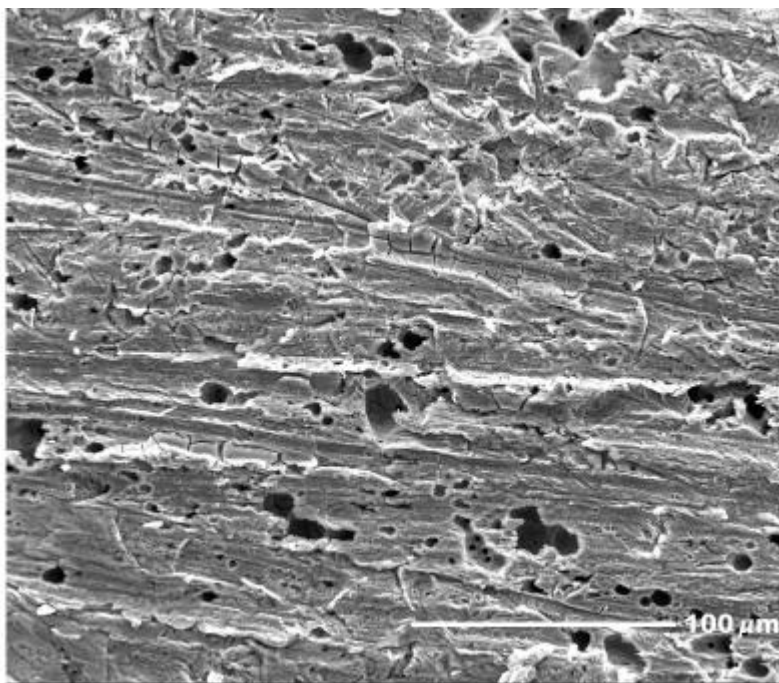


Figure 13(h): SEM micrograph of Fe (*rough, P120*) after one hour of immersion in 0.1 M HCl + 0.01 M Na₂MoO₄ followed by an applied potential of 1000 mV above E_c for 60 seconds.

The arrows in the figure point to some of the crystallographic pits. The presence of MoO₄²⁻ did not eliminate pitting-related corrosion. The latter could be attributed to the relatively high anodic potential. However, it seems to change the pits' morphologies, sizes, and number when the pits were covered by corrosion products.

4. CONCLUSIONS

4.1 The corrosion rate of Fe increases with increasing surface roughness in 0.1 M HCl and in 0.1 M H₂SO₄ in both MoO₄²⁻ absence and presence.

4.2 The effects of surface roughness on the Fe corrosion rate are more apparent in 0.1 M HCl than 0.1 M H₂SO₄ solutions.

4.3 The presence of MoO₄²⁻ increases the corrosion rate of Fe in 0.1 M HCl and 0.1 M H₂SO₄.

4.4 Stable pits form under high anodic polarization in 0.1 M HCl in both MoO₄²⁻ absence and presence.

4.5 The pits are randomly distributed and look crystallographic.

4.6 Surface roughness appears to affect the nature of the double layer as indicated by its effect on the value of α .

4.7 The CPE can be considered to act as a capacitor in H₂SO₄ but not in HCl.

ACKNOWLEDGMENT

The authors would like to express their sincere appreciation to the Research Affairs at the United Arab Emirates University (UAEU) for their partial support of this project. The authors would also like to express their gratitude to the department of chemistry at the UAEU for providing the facilities to carry out this project.

References

1. V. S. Sastri, *Green Corrosion Inhibitors*, John Wiley and Sons, New Jersey (2011).
2. A. J. Sedriks, *Corrosion of Stainless Steels*, 2nd ed., John Wiley and Sons, Inc. (1996).
3. J. R. Ambrose, *Corrosion*, 34 (1978) 27.
4. T. Kodama and J. R. Ambrose, *Corrosion*, 33 (1977) 155.
5. K. Sugimoto and Y. Sawada, *Corrosion*, 32 (1976) 347.
6. C. R. Clayton and Y. C. Lu, *Corrosion Science*, 29 (1989) 881.
7. S. Virtanen, B. Surber and P. Nylund, *Corrosion Science*, 43 (2001) 1165.
8. A. Pardo, M. C. Merino, A. E. Coy, F. Viejo, R. Arrabal, and E. Matykina, *Corrosion Science*, 50 (2008) 780.
9. Ahmed S. Alshamsi, *International Journal of Basic and Applied Sciences*, 2 (2013) 303.
10. S. A. M. Refaey, *Applied Surface Science*, 240 (2005) 396.
11. Xianghong Li, Shuduan Deng, and Hui Fu, *Corrosion Science*, 53 (2011) 2748.
12. M. R. Ali, C. M. Mustafa, and M. Habib, *Journal of Scientific Research*, 1 (2009) 82.
13. Ahmed S. Alshamsi, *Int. J. Electrochem. Sci.*, 8 (2013) 591.
14. G. O. Ilevbare and G. T. Burstein, *Corrosion Science*, 45 (2003) 1545.
15. H. S. Isaacs and S.-M. Huang, *J. Electrochemical Soc.*, 143 (1996) L277.
16. H. Wang, J. Xie, K.P. Yan, M. Duan, and Y. Zou, *Corrosion Science*, 51 (2009) 181.
17. G. T. Burstein and P. C. Pistorius, *Corrosion*, 51 (1995) 380.
18. Deepak Dwivedi, Katerina Lepkova, and Thomas Becker, *RSC Adv.*, 7 (2017) 4580.
19. Hai-bo Wang, Yun Li, Guang-xu Cheng, Wei Wu, Yao-heng Zhang, and Xin-yun Li, *Int. J. Electrochem. Sci.*, 13 (2018) 5268.
20. Viera Zatkalíková, Monika Oravcová, Peter Palček, and Lenka Markovičová, *TRANSACTIONS OF FAMENA*, XLI-4 (2017) 25.
21. A. S. Toloei, V. Stoilov, and D. O. Northwood, *WIT Transactions on Engineering Sciences*, 90 (2015) 355.
22. Roxanna B. Alvarez, Holly J. Martin, M.F. Horstemeyer, Mei.Q. Chandler, Neil Williams, Paul T. Wang, and Augusto Ruiz, *Corrosion Science*, 52 (2010) 1635.
23. S. Sathiyarayanan, C. Jeyaprabha, S. Muralidharan, and G. Venkatachari, *Applied Surface Science*, 252 (2006) 8107.
24. S. Ben Aoun, M. Bouklah, K. F. Khaled, and B. Hammouti, *Int. J. Electrochem. Sci.*, 11 (2016) 7343.
25. Z. Zhang, S. Chen, Y. Li, S. Li, and L. Wang, *Corrosion. Science*, 51 (2009) 291.